

Hybrid black-hole binary initial data

Bruno C. Mundim¹, Bernard J. Kelly^{2,3}, Yosef Zlochower¹,
Hiroyuki Nakano¹, Manuela Campanelli¹

¹ Center for Computational Relativity and Gravitation, School of Mathematical Sciences, Rochester Institute of Technology, Rochester, New York 14623, USA

² CRESST & Gravitational Astrophysics Laboratory, NASA/GSFC, 8800 Greenbelt Rd., Greenbelt, MD 20771, USA

³ Dept. of Physics, University of Maryland, Baltimore County, 1000 Hilltop Circle, Baltimore, MD 21250, USA

E-mail: bcmsma@astro.rit.edu, bernard.j.kelly@nasa.gov,
yosef@astro.rit.edu, nakano@astro.rit.edu, manuela@astro.rit.edu

Abstract. Traditional black-hole binary puncture initial data is conformally flat. This unphysical assumption is coupled with a lack of radiation signature from the binary's past life. As a result, waveforms extracted from evolutions of this data display an abrupt jump. In Kelly *et al* [1], a new binary black-hole initial data with radiation contents derived in the post-Newtonian (PN) calculation was adapted to puncture evolutions in numerical relativity. This data satisfies the constraint equations to the 2.5PN order, and contains a transverse-traceless “wavy” metric contribution, violating the standard assumption of conformal flatness. Although the evolution contained less spurious radiation, there were undesired features; the unphysical horizon mass loss and the large initial orbital eccentricity. Introducing a hybrid approach to the initial data evaluation, we significantly reduce these undesired features.

PACS numbers: 04.25.Dm, 04.25.Nx, 04.30.Db, 04.70.Bw

Submitted to: *Class. Quantum Grav.*

1. Introduction

The field of Numerical Relativity (NR) has progressed at a remarkable pace since the breakthroughs of 2005 [2, 3, 4] with the first successful fully non-linear dynamical numerical simulation of the inspiral, merger, and ringdown of an orbiting black-hole binary (BHB) system. In particular, the “moving-punctures” approach, developed independently by the NR groups at NASA/GSFC and at RIT, has now become the most widely used method in the field and has been successfully applied to evolve generic BHBs. This approach regularizes a singular term in the space-time metric and allows the black holes (BHs) to move across the computational domain. Since this breakthrough, BHB physics has rapidly matured into a critical tool for gravitational wave (GW) data analysis and astrophysics. Recent developments include: studies of the orbital dynamics of spinning BHBs [5, 6, 7, 8, 9, 10, 11], calculations of recoil velocities from the merger of unequal-mass BHBs [12, 13, 14], the surprising discovery that very large recoils can be acquired by the remnant of the merger of two spinning BHs [15, 16, 17, 18, 19, 20, 21, 22, 23, 24, 25, 26, 27, 8, 28, 29, 30], empirical models relating the final mass and spin of the remnant with the spins of the individual BHs [31, 32, 33, 34, 35, 36, 37, 38], and comparisons of waveforms and orbital dynamics of BHB inspirals with post-Newtonian (PN) predictions [39, 40, 41, 42, 43, 44, 45, 46, 47].

One of the important applications of NR is the generation of waveforms to assist GW astronomers in their search and analysis of GWs from the data collected by ground-based interferometers, such as LIGO [48] and VIRGO [49], and future missions, such as LCGT [50], LISA [51], ET [52] and DECIGO [53]. BHBs are particularly promising sources, with the final merger event producing a strong burst of GWs at a luminosity of $L_{GW} \sim 10^{22} L_{\odot} \ddagger$, greater than the combined luminosity of all stars in the observable universe. The central goal of the field has been to develop the theoretical techniques, and perform the numerical simulations, needed to explore the highly dynamical regions and thus generate GW signals from a representative sample of the full BHB parameter space. Accurate waveforms are important to extract physical information about the binary system, such as the masses of the components, BH spins, and orientation.

With this in mind, we note a drawback shared by most present-day comparable-mass black-hole binary simulations in three spatial dimensions: they are performed using conformally flat initial data given by the Bowen-York (BY) [54] prescription as applied by Brandt and Brügmann [55]. This prescription, while numerically convenient, lacks physical realism. The unique stationary vacuum black-hole solution to Einstein’s equations is the Kerr solution, which is not conformally flat for non-zero spin. We cannot approximate this with single-puncture spinning BY data without also including unphysical radiation.

Conversely, approximating an inspiralling black-hole binary system with two-puncture BY data will leave out the gravitational radiation expected in physical

\ddagger This luminosity estimate is independent of the binary mass and takes into account that 3 – 10% of the total mass M of the binary is radiated over a time interval of $\sim 100M$ [38].

situations – radiation inextricably linked to the past history that produced the inspiral. This is demonstrated in plots of extracted radiation from current simulations, where observers a distance R_{ext} from the binary only see a flat radiation profile for the first $t \approx R_{\text{ext}}$ of evolution time.

The post-Newtonian (PN) initial data developed in this and preceding papers [56, 57, 1] is an attempt to address this shortcoming in initial data by incorporating to leading PN accuracy the gravitational-wave content of a physical binary inspiral. The previous paper in this series, [57], demonstrated the evolution behaviour of the data evolved with no numerical conditioning of the constraints. In summary, we noted that the extracted radiation agreed with physical expectations from the very start of the simulation (though the burst of junk radiation associated with puncture evolutions was not completely removed). We also encountered several related weaknesses in the new evolved data, including:

- very high eccentricity ($\sim 10\%$) in puncture trajectories, until around $100M$ before merger;
- (possibly related) an extremely slow stabilization of pre-merger horizon masses during evolution;
- large constraint violations when all the gravitational-wave terms are included.

In this paper, we present hybrid BY-PN data with partial constraint conditioning, aimed at resolving these issues.

In Section 2, we summarize the standard conformally flat Bowen-York puncture initial data. In Section 3, we review the theoretical work that led to the PN data, and discuss the encoding of the past history of the binary in Section 4. In Section 5, we present the new hybrid initial data, and demonstrate its improved numerical behaviour. The numerical evolutions and comparison for various initial data are discussed in Section 6. We conclude in Section 7 with a discussion of future development and application of this data.

2. BY Initial Data

Most groups use the puncture prescription of Brandt and Brügmann [55] with Bowen-York extrinsic curvature [54] to initialize the numerical fields for a puncture evolution. In this prescription, the three-metric γ_{ij} is conformally flat:

$$\gamma_{ij} = \psi^4 \delta_{ij}, \quad (1)$$

and the conformal factor ψ must satisfy the Hamiltonian constraint

$$\Delta\psi + \frac{1}{8} K^{ij} K_{ij} \psi^{-7} = 0, \quad (2)$$

where the conformal Bowen-York extrinsic curvature K_{ij} already satisfies the momentum constraint for holes with arbitrary momentum and spin. Brandt and Brügmann’s insight

to find the solution to equation (2) was to factor out the divergent parts of ψ , leaving a well-behaved, simply-connected sheet on which to solve their modified constraint:

$$\psi_{\text{BY}} = 1 + \sum_{a=1}^2 \frac{m_a}{2r_a} + u, \quad (3)$$

where BY refers hereafter to Bowen-York puncture data, $r_a = |\mathbf{x} - \mathbf{x}_a|$, and m_a and \mathbf{x}_a denote the “bare” mass and location of each hole, respectively. In this prescription, only a single elliptic equation for u has to be solved, and u will be regular everywhere on the grid. Despite the great success in simplifying the form of the constraint equations, this prescription does *not* make use of any information to accurately describe the past evolution of the binary black holes. Conformal flatness, for example, prevents the astrophysically expected gravitational radiation from being included in the initial data.

3. PN Initial Data in ADM-TT Gauge

Post-Newtonian (PN) techniques are considered to *accurately* represent an astrophysical system in the limit of slow motion/far-apart black holes. See Blanchet [58] and Schäfer [59] for a review of the PN approach.

In the canonical Hamiltonian formulation with point-like sources in general relativity, Ohta *et al* [60, 61, 62] investigated a class of coordinate systems in which the metric tensor becomes Minkowskian at spatial infinity, and developed the 2PN order calculation. In particular, they found a compact way of expressing a compatible coordinate condition with the aid of the ADM formalism. By applying a transverse-traceless decomposition of the three-metric and its conjugate momentum, they were able to encode the full information about the dynamics of the canonical fields and particle variables in a reduced Hamiltonian, which is obtained by solving the constraint equations *only*. To solve the constraints, we follow the steps of Schäfer [63]. Historically, the 2PN order calculation was completed by Damour and Schäfer [64]. Shortly afterward, Schäfer [63, 65] included the 2.5PN radiation-reaction terms in this Hamiltonian approach.

Tichy *et al* [56] adapted the 2.5PN ADM-TT results to puncture initial data for numerical relativity. We start then from the PN expression for the spatial metric, which differs from conformally flatness by a radiative term h_{ij}^{TT} :

$$\gamma_{ij}^{\text{PN}} = \psi_{\text{PN}}^4 \delta_{ij} + h_{ij}^{\text{TT}}, \quad (4)$$

where the PN conformal factor is given by

$$\psi_{\text{PN}} = 1 + \sum_{a=1}^2 \frac{E_a}{2r_a} + O(\epsilon^6), \quad (5)$$

where $\epsilon \equiv 1/c$ is the PN order parameter and

$$E_a = \epsilon^2 m_a + \epsilon^4 \left(\frac{\mathbf{P}_a^2}{2m_a} - \frac{m_1 m_2}{2r_{12}} \right). \quad (6)$$

Here, \mathbf{p}_a represents the linear momentum of each hole, and r_{12} is the separation between the holes.

The accompanying extrinsic curvature K_{ij}^{PN} is related to the three-metric's (trace-free) conjugate momentum π_{PN}^{ij} :

$$\pi_{\text{PN}}^{ij} = \frac{1}{\psi_{\text{PN}}^4} \left(\epsilon^3 \pi_{(3)}^{ij} + \epsilon^5 \pi_{(5)}^{ij} \right) + O(\epsilon^6). \quad (7)$$

(See the complete equation (17) in [56].) Explicit expressions for $\pi_{(3)}^{ij}$ and $\pi_{(5)}^{ij}$ can be found in [66]; The leading-PN-order term, $\pi_{(3)}^{ij}$, coincides with the standard Bowen-York linear-momentum contribution for a nonspinning binary.

Near each particle, the spatial metric can be approximated by:

$$\gamma_{ij}^{\text{PN}} \sim \left(1 + \frac{E_a}{2r_a} \right)^4 \delta_{ij} + O(1/r_a^3), \quad (8)$$

which is just the Schwarzschild metric in isotropic coordinates. For $r_a \rightarrow 0$, the coordinate singularity is approached. This represents the inner asymptotically flat end of the Schwarzschild metric in isotropic coordinates, or the puncture representation of the Schwarzschild solution. This shows that if the metric form is kept as in equation (4), then there is a black hole centred on each particle.

The traceless-transverse part of the spatial three-metric, on the other hand, can be constructed by imposing an outgoing wave condition. We can rewrite the evolution equation for h_{ij}^{TT} as:

$$h_{ij}^{\text{TT}} = -\square_{\text{ret}}^{-1} \delta_{ij}^{\text{TT}kl} \left[\sum_{a=1}^N \frac{p_{ak} p_{al}}{m_a} \delta(x - x_a) + \frac{1}{4} \phi_{,k}^{(2)} \phi_{,l}^{(2)} \right], \quad (9)$$

where $\delta_{kl}^{\text{TT}ij}$ is the TT-projection operator as defined in [63]. Schäfer [63] suggested a “near zone” approximation for h_{ij}^{TT} , by splitting the retarded inverse d'Alembertian in (9) with an inverse Laplacian:

$$\begin{aligned} h_{ij}^{\text{TT}} &= -[\Delta^{-1} + (\square_{\text{ret}}^{-1} - \Delta^{-1})] \delta_{ij}^{\text{TT}kl} [\cdot \cdot \cdot] \\ &= h_{ij}^{\text{TT}(\text{NZ})} + h_{ij}^{\text{TT}(\text{remainder})} + O(\epsilon^5). \end{aligned} \quad (10)$$

The explicit form of this near-zone (NZ) approximation was given by Jaranowski and Schäfer [66]. A few years later, Kelly *et al* [57] completed the picture for nonspinning black holes by determining the “remainder” TT term, $h_{ij}^{\text{TT}(\text{remainder})}$ to 2PN order. The structure of the remainder term divides into three segments, according to time of evaluation:

$$h_{ij}^{\text{TT}(\text{remainder})} = h_{ij}^{\text{TT}(\text{present})} + h_{ij}^{\text{TT}(\text{retarded})} + h_{ij}^{\text{TT}(\text{interval})}. \quad (11)$$

For each field point where h_{ij}^{TT} is to be evaluated, the “present” term is evaluated using the particle positions and momenta at $t = 0$. The “retarded” term is evaluated using positions and momenta at the retarded time of each source particle relative to the field point. The “interval” term is an integral over the particles' paths from the retarded time to the present.

The present-time piece almost completely *cancels* the near-zone solution. The kinetic terms (i.e., those involving particle momenta) cancel exactly, while potential terms (those involving particle-pair separations) are strongly suppressed. The retarded-time piece reduces to the quadrupole solution for a nonspinning binary as $r_{12}/r \rightarrow 0$ where r denotes the field distance. The interval piece is too difficult to do in generality: we must integrate numerically.

The ADM-TT data introduced here has several attractive properties, which we briefly restate here. The three-metric and extrinsic curvature expressions are easily found. Unlike harmonic coordinates, ADM-TT has no logarithmic divergences. For a single BH, the data reduces to the Schwarzschild metric in isotropic coordinates. Up to 1.5PN order, the data coincides with the (unsolved) puncture approach – conformally flat, with Bowen-York extrinsic curvature. The trace of the extrinsic curvature vanishes up to 3PN order. The Hamiltonian constraint decouples from the momentum constraints.

4. Encoding the Past History of the Binary

To evaluate this initial data for a given separation at $t = 0$, we must know not only the particle momenta at $t = 0$, but also the position and momentum of each particle over the past history of the binary, at least from the retarded time relative to the most distant grid point in the numerical domain. That is, the larger the numerical domain, the further back in time we must look for the information needed to fill in the h_{ij}^{TT} fields at these spatially distant points.

To supply this position and momentum information, we evolve the Hamiltonian equations of motion, using a standard Taylor PN Hamiltonian and flux function evaluated at 3PN and 3.5PN order, respectively. The set of equations which we use in this paper has been given in [67]. This evolution is started at a suitably large separation ($r_{12} \sim 40M$ is easily sufficient for current purposes), and the separation and orbital phase are saved for later interpolation. We then apply a shift in time and orbital frequency to match the initial conditions of the fully numerical evolution.

This shifted trajectory data is used directly to evaluate the present-time fields. We also use it to evaluate the two retarded times (one for each particle) at each field point by a nonlinear Newton-search algorithm. Then we can evaluate the retarded-time fields, and numerically integrate the interval terms.

5. Hybrid Initial Data

The similarities of the wavy ADM-TT leading-order terms and the Bowen-York puncture data may be the key to further constraining the initial data. We use the rationale that the largest Hamiltonian violation contributions are due to the PN conformal factor, ψ_{PN} , since h_{ij}^{TT} is relatively much smaller for field points closer to the punctures. We propose then a hybrid initial data prescription in which we first solve the Hamiltonian constraint

for the traditional Bowen-York puncture initial data and then rescale and superpose the higher-order PN terms to this solution. More specifically, the Bowen-York extrinsic curvature is used as usual to source the Hamiltonian constraint for a conformally flat spatial metric:

$$\Delta\psi_{\text{BY}} + \frac{1}{8}K_{\text{BY}}^{ij}K_{ij}^{\text{BY}}\psi_{\text{BY}}^{-7} = 0. \quad (12)$$

The solution follows then from the puncture trick and is given by

$$\psi_{\text{BY}} = 1 + \frac{1}{2}\left(\frac{m_1}{r_1} + \frac{m_2}{r_2}\right) + u, \quad (13)$$

where u , the regular part of the solution, is determined by the numerical solution of the resulting Poisson-like elliptic equation. The functional similarity of this solution to the one provided by the PN expansion, equation (5), is quite striking. The singular part, or the Brill-Lindquist part [68] if you wish, has the same functional form in each case, differing only in how the bare masses of particles and black holes are treated, and the missing regular contribution u in the PN conformal factor. In this new approach the ADM canonical quantities are then rescaled by the Bowen-York solution, ψ_{BY} , instead of the PN conformal factor ψ_{PN} :

$$\gamma_{ij} = \psi_{\text{BY}}^4 \delta_{ij} + h_{ij}^{\text{TT}}, \quad (14)$$

$$\pi^{ij} = \frac{1}{\psi_{\text{BY}}^4} \left(\epsilon^3 \pi_{(3)}^{ij} + \epsilon^5 \pi_{(5)}^{ij} \right), \quad (15)$$

where we note that $\pi_{(3)}^{ij}$ corresponds exactly to the spinless Bowen-York contribution. The transverse-traceless part of the metric, h_{ij}^{TT} , and the higher-order PN contribution to the conjugate momentum, $\pi_{(5)}^{ij}$, are then superposed with this puncture data.

5.1. Constraint violations

Looking into the violation of the constraint equations, Fig. 1, it becomes clear that the PN metric becomes inaccurate close to the punctures, at least when compared to the traditional Bowen-York data. The long-dash-dotted brown curve there represents the constraint violation for the PN metric in the ADM-TT gauge, labeled in the figure and in all plots hereafter as “ADMTT PN”. The purple vertical dotted lines indicate the apparent horizon location around one of the punctures; here the one located on the y -axis at $y=-4M$. Focusing our attention on the plot on the left panel, the Hamiltonian constraint violation, we can observe a negative violation outside of the horizon for the PN data. This can be interpreted as, and has the effect of, an unphysical negative mass gravitating around each black hole. Unfortunately, the hybrid approach just introduced in the last section did not reduce this violation considerably, as the green dashed line in the plot shows. We decided then to investigate a way to improve the data approximation closer to the apparent horizons and that led to the second crucial element of the approach proposed here: the use of attenuation functions.

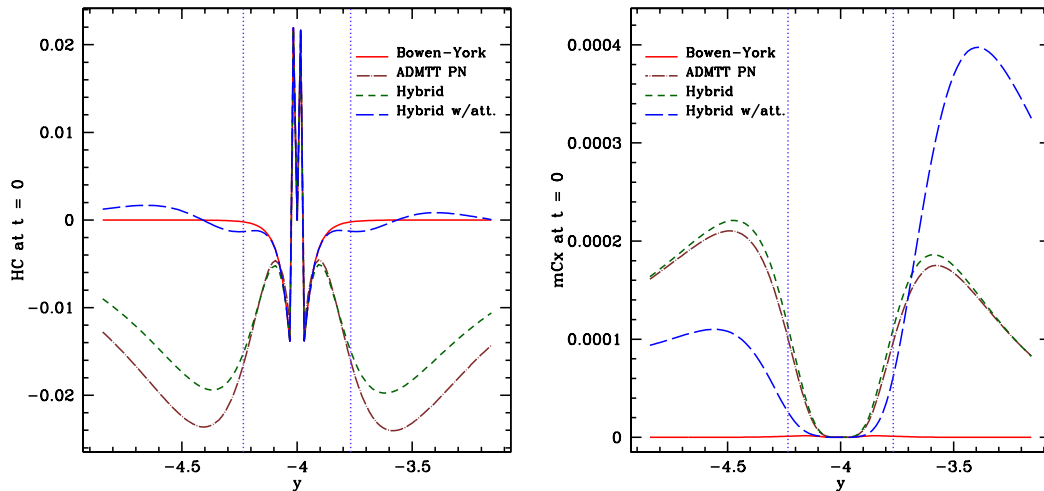


Figure 1. Constraint violations. These figures compare the violation of the constraint equations around a puncture located in the y -axis at $y = -4M$. The (purple) dotted vertical lines indicate the location of the apparent horizon. The (red) solid line represents the violation for the traditional Bowen-York data. The long-dash-dotted (brown) lines describes the violation for the ADM-TT PN data, while the (green) dashed and the (blue) long-dashed lines correspond to the Hybrid and Hybrid with attenuation function, respectively. We keep the line styles consistently the same in all figures hereafter to facilitate comparison. The plot on the left panel represents the Hamiltonian constraint violation and the one on the right represents the momentum constraint violation.

5.2. Attenuation function

Since the PN approximation of the metric and extrinsic curvature is inaccurate for the inner or internal zone, i.e., the region around each black hole in binary systems where $r_1 \ll r_{12}$ and $r_2 \ll r_{12}$, we need to consider a different approach to construct the initial data around that region. Johnson-McDaniel, Yunes, Tichy and Owen [69] introduced the black hole perturbation calculation by Detweiler [70] to be used as an approximation for the inner zone.

Here, we treat the inner-zone metric by a simpler approach. We discard the PN contribution around each black hole by applying an attenuation function defined as follows (see Fig. 2 for its functional form along an interval on the y -axis):

$$\begin{aligned} \mathcal{F} &= \frac{1}{4} \left[\tanh \left(\ln \left(\frac{r_1}{a_t m_1} \right) \right) + 1 \right] \left[\tanh \left(\ln \left(\frac{r_2}{a_t m_2} \right) \right) + 1 \right] \\ &= \left(1 + \frac{a_t^2 m_1^2}{r_1^2} \right)^{-1} \left(1 + \frac{a_t^2 m_2^2}{r_2^2} \right)^{-1}, \end{aligned} \quad (16)$$

where a_t is a constant parameter[§]. Our hybrid initial data approach with the use of an

[§] Note that when we apply this attenuation function to h_{ij}^{TT} , the correction at large distances is at higher PN order than we treat in this paper. At large distances, we a Taylor expansion with respect

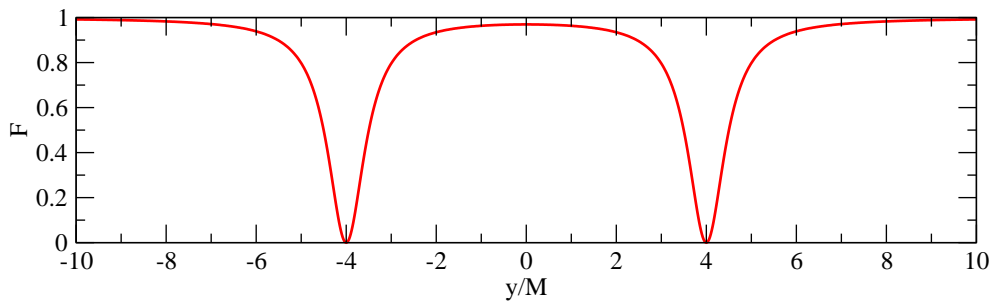


Figure 2. The attenuation function along the y axis for a binary with $m_1 = m_2 = M/2$ at $y_1 = -y_2 = 4M$, and $a_t = 1$.

attenuation function then becomes:

$$\gamma_{ij} = \psi_{\text{BY}}^4 \delta_{ij} + \mathcal{F} h_{ij}^{\text{TT}}, \quad (18)$$

$$\pi^{ij} = \frac{1}{\psi_{\text{BY}}^4} \left(\epsilon^3 \pi_{(3)}^{ij} + \mathcal{F} \epsilon^5 \pi_{(5)}^{ij} \right). \quad (19)$$

The effect of this procedure is a considerable reduction of the Hamiltonian constraint violation, as the blue long-dashed curve indicates on the left panel of Fig. 1.

While the Hamiltonian constraint violation is improved, and we are going to discuss its effect on the data evolution later on, the momentum constraint violation seems to be unaffected by these two key ingredients of our procedure. Both the Hybrid and the Hybrid data with attenuation seem to affect the momentum constraint residuals negligibly when compared to the PN data. We are also going to discuss later how we think this may be affecting the data evolution. But before discussing any further properties of this data, let us say a few words on how the numerical experiments were prepared and performed. This is the topic of the next section.

6. Numerical Evolution

The black-hole binary studied in these experiments had a mass ratio of $q = 1$, was nonspinning, with punctures initially located on the y -axis at $\pm 4M$. In this framework we use the puncture approach [55] along with the TWO PUNCTURES thorn [71] to calculate the Bowen-York initial data. We evolved these black-hole-binary data-sets using the LAZEV [72] implementation of the moving puncture formalism [3, 4] with the conformal factor $W = \sqrt{\chi} = \exp(-2\phi)$ suggested by [10] as a dynamical variable. For the runs presented here we use centred, eighth-order finite differencing in space [73] and an RK4 time integrator (note that we do not upwind the advection terms).

to m_i/r_i (i.e., a PN expansion) yields

$$\mathcal{F} h_{ij}^{\text{TT}} = h_{ij}^{\text{TT}} \left(1 - \frac{a_t^2 m_1^2}{r_1^2} - \frac{a_t^2 m_2^2}{r_2^2} + \dots \right). \quad (17)$$

Therefore, the corrections due to the attenuation function are at 2PN higher order than the leading order of h_{ij}^{TT} .

We obtain accurate, convergent waveforms and horizon parameters by evolving this system in conjunction with a modified 1 + log lapse and a modified Gamma-driver shift condition [74, 3], and an initial lapse $\alpha(t = 0) = 2/(1 + \psi_{\text{BL}}^4)$. The lapse α and shift β^a are evolved with

$$\begin{aligned} (\partial_t - \beta^i \partial_i) \alpha &= -2 \alpha K, \\ \partial_t \beta^a &= \frac{3}{4} \tilde{\Gamma}^a - \eta \beta^a, \end{aligned} \tag{20}$$

where η is constant.

We use the Cactus/Einstein Toolkit code [75, 76] to provide the parallel infrastructure and the Carpet [77] mesh refinement driver to provide a ‘moving boxes’ style mesh refinement. In this approach refined grids of fixed size are arranged about the coordinate centers of both holes. The Carpet code then moves these fine grids about the computational domain by following the trajectories of the two black holes.

We use the AHFINDERDIRECT thorn [78] to locate apparent horizons. We measure the magnitude of the horizon spin S using the Isolated Horizon algorithm detailed in [79]. Once we have the horizon spin, we can calculate the horizon mass M_{AH} via the Christodoulou formula [80]:

$$M_{\text{AH}} = \sqrt{M_{\text{irr}}^2 + \frac{S^2}{4 M_{\text{irr}}^2}}, \tag{21}$$

where $M_{\text{irr}} = \sqrt{A/(16\pi)}$ is the *irreducible mass* and A is the surface area of the horizon.

For the runs in this paper, we used a grid hierarchy spanning nine levels of refinement. We ran three different sets of grid hierarchy resolutions in order to determine the waveform accuracy, shown in Fig. 3. The low-, medium- and high-resolution hierarchies have mesh spacings of $h_c = \{5M, 4M, 3.2M\}$ for the coarsest grid and of $h_f = \{M/51.2, M/64, M/80\}$ for the finest ones, respectively. The mesh spacings in the wave-extraction region are $h_{\text{ext}} = \{1.25M, 1M, 0.8M\}$. We apply reflection-boundary symmetry at the $z = 0$ plane and π symmetry (that is, particle-exchange symmetry) at the $x = 0$ plane. The outer boundary is located at $400M$.

The results comparing the different initial data sets, presented in the following sections, used the medium grid hierarchy only, i.e., the finest mesh spacing for this hierarchy is $h_f = M/64$, resulting in approximately 30 grid points across the initial apparent horizon.

6.1. Apparent Horizon Mass

The first result from the evolution of the data introduced in the previous section that we would like to discuss concerns the apparent horizon mass. It was reported earlier [1] for the PN data that the mass was not being conserved with time – some sort of mass ‘leak’ was plaguing the data evolution. We confirm this problem in Fig. 4, as we can observe the long time it takes for the PN irreducible mass to relax towards a constant value.

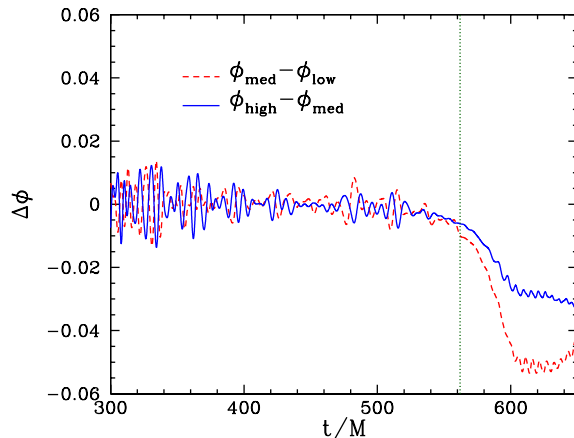


Figure 3. Phase accuracy. This figure shows the difference in phase for the $(2, 2)$ mode of the radiative Weyl scalar ψ_4 at different resolutions. We compare the difference of the medium and low resolutions with that of the high and medium ones. We see that the phase error is below the threshold of 0.05 at $M\Omega = 0.2$ (vertical dotted green line) suggested by the NRAR collaboration [81].

The first step we took when trying to tackle this issue was to introduce the attenuation function for the PN data. As the purple dotted curve in the figure reveals, this approach alone was not successful. Only when we introduced the hybrid approach to the binary black-hole initial data, did we see an improvement in this unwanted feature. Now the mass conservation seems much more accurate, left only the presence of some bumps in the curve.

We believe that the presence of these bumps in the data are related to unphysical negative mass, resulting from the initial Hamiltonian constraint violation. Since these bumps appear approximately every half orbital period, or roughly when the punctures cross the y -axis, it may be reasonable to assume that the initial Hamiltonian violations hangs in the domain around their initial locations or in the holes’ “wakes”, occasionally being absorbed by the passing hole. The attenuation function seems to reduce this effect slightly, however only when associated with the hybrid data.

6.2. Eccentricity

Several methods have been proposed to estimate the eccentricity of numerically evolved binary inspirals; for recent examples, see [39, 82, 83]. We estimate the eccentricity of all four different data sets by first χ^2 -fitting a polynomial function, $r_{\text{fit}}(t)$, to the binary coordinate separation, $r_{\text{NR}}(t)$, as a function of time. We subtract then the numerical data from the fitted function and normalize it by the same fitted function:

$$e_r(t) = \frac{r_{\text{NR}}(t) - r_{\text{fit}}(t)}{r_{\text{fit}}(t)} \simeq e_r \cos(\Omega_r t + \phi_0). \quad (22)$$

The interpolating polynomial must be monotonically decreasing with no extrema in the fitting interval. We use the highest possible polynomial order satisfying these

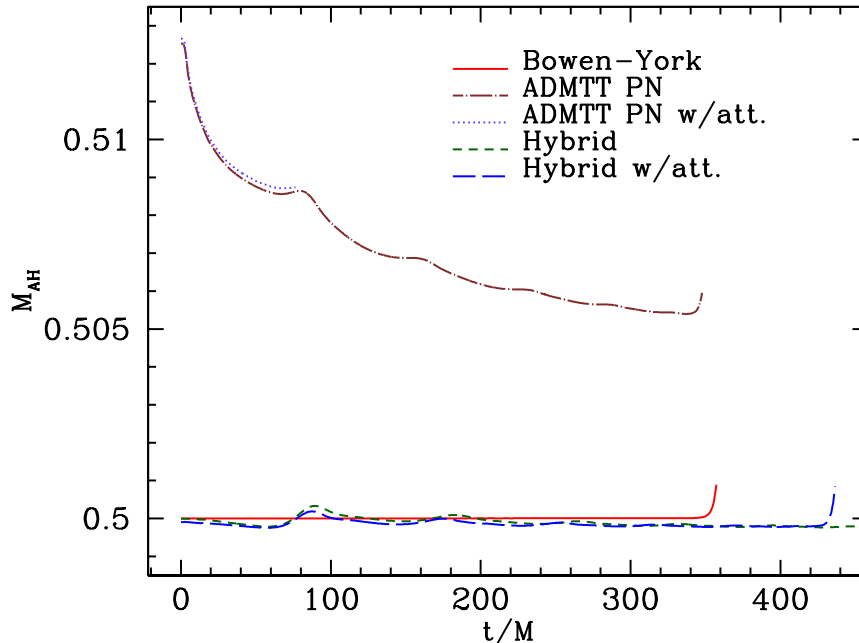


Figure 4. The behaviour of each hole’s apparent horizon mass M_{AH} for Bowen-York, ADM-TT PN, ADM-TT PN with attenuation [(purple) dotted line], Hybrid and Hybrid with attenuation initial data. The mass “leak” was reduced considerably with the hybrid initial data.

constraints. The assumption behind this procedure is a secular quasi-adiabatic shrinking of the orbital separation. The amplitude of the sinusoidal part extracted out of this orbital decay provides then an estimate of the orbital eccentricity.

Specifically for these runs, where the initial separation is $r_0 = 8M$, we fit a second-order polynomial curve to the numerical data. We were careful to choose a time to stop fitting much earlier than the coalescence time. Usually we would eliminate the initial gauge effects from the data, and start fitting somewhere around $t = 40M$ or later, as was the case for both instances of Hybrid data presented in Fig. 5. However this procedure turned out to be very sensitive to the initial fit separation for the Bowen-York and PN data. We decided then to include this initial transient in order to establish only an upper bound estimate for the eccentricity. We believe that this is not necessary for binaries initially farther apart.

Amplitude readings from the eccentricity estimator plot as well as from a bare inspection of the coordinate separation as a function of time, Fig. 5, indicate that the Bowen-York data has an eccentricity of the order of 10^{-2} . Clearly the PN eccentricity is around 5 times this value. The Hybrid data alone, on the other hand, did not have a considerable impact on the eccentricity, possibly due to the fact that the momentum constraint violations were not improved as well. We could minimize a bit the high eccentricity effects by introducing the attenuation function, but this problem remains open.

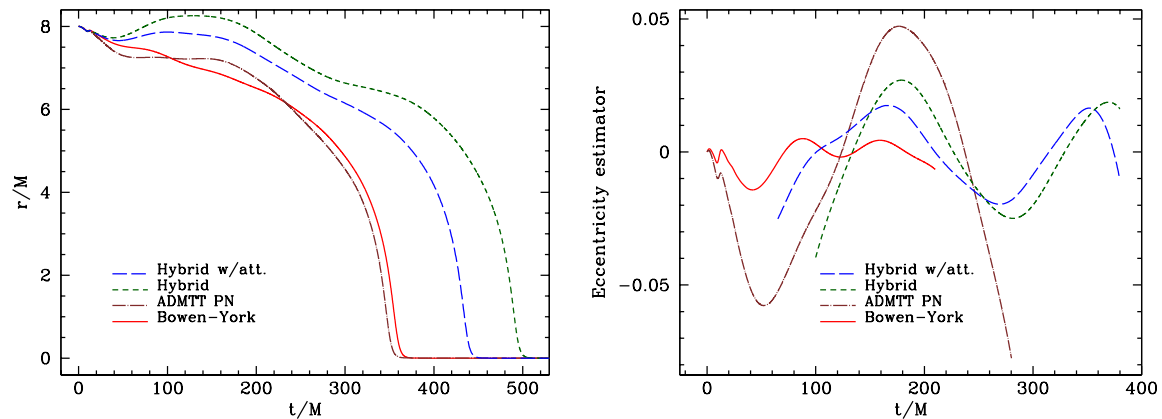


Figure 5. Coordinate separation (left panel) and its eccentricity estimator in equation (22) (right panel) versus time for Bowen-York, ADM-TT PN, Hybrid and Hybrid with attenuation initial data.

6.3. Waveforms

We illustrate in Fig. 6 the presence of the realistic wave content in the hybrid initial data. The figure shows the $z = 0$ slice of the data for the real part of the Weyl scalar ψ_4 multiplied by the areal radius R_{areal} . We show the traditional Bowen-York data for comparison in the right panel of the same figure.

Like the wavy ADM-TT PN data, the hybrid data significantly reduces the amplitude of the spurious radiation when compared to the traditional Bowen-York data as is demonstrated in Fig. 7 for the real and imaginary parts of the $(2, 2)$ mode of the Weyl scalar ψ_4 . In Fig. 8 we compare the amplitude (left panel) and phase (right panel) of this mode. We can observe a clear reduction in the amplitude and a dramatic improvement in the phase for all cases compared to Bowen-York data. Note that there is a decrease in amplitude for the Hybrid data, suggesting the binary is cast into a larger orbital separation. The use of attenuation function greatly reduces this effect, however. For the $(4, 4)$ mode we only achieve a visible reduction of the junk radiation in the amplitude with the Hybrid with attenuation data, Fig. 9, which suggests that we need to improve the analytical approximation of the ADM canonical quantities in the inner zone if we want to accurately describe black-hole tidal effects. The disturbances in phase still seem greatly reduced.

6.4. Final State

Finally, we would like to comment on another advantage of the Hybrid data over the PN data. As Fig. 10 shows, the final state of the Hybrid data is much closer to the Bowen-York data than the PN one. Additionally, the post-merger horizon mass shows a significantly larger drift over time for the PN data than for the Hybrid data.

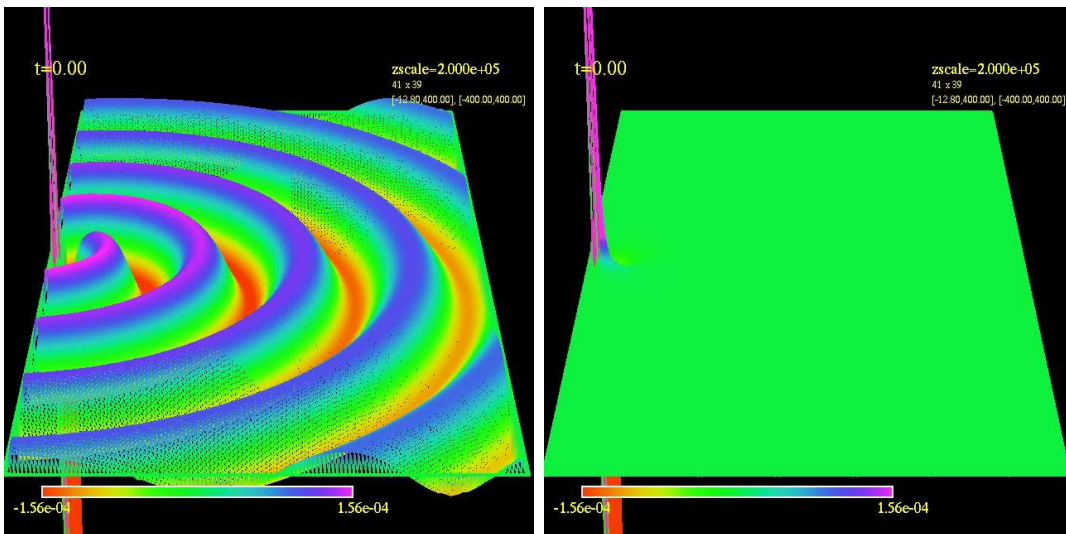


Figure 6. Comparison between the wavy pattern at $t = 0$ present in $R_{\text{areal}} \mathcal{R}e(\psi_4)$ for the hybrid initial data (left) and the traditional Bowen-York data (right).

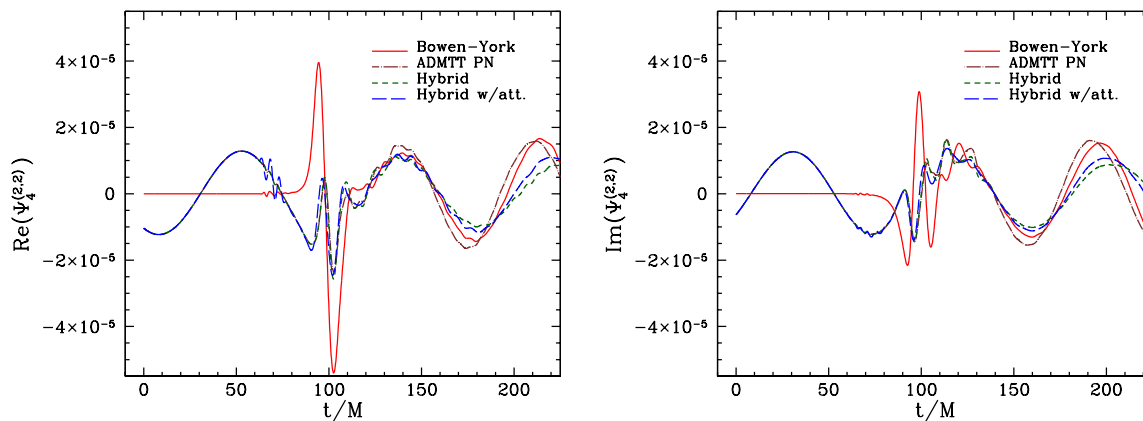


Figure 7. Real and imaginary parts of the $(2, 2)$ mode of the Weyl scalar ψ_4 resulting from the evolution of Bowen-York, ADM-TT PN, Hybrid and Hybrid with attenuation initial data. The extraction radius is $R_{\text{ext}} = 90M$.

7. Conclusion

Motivated by the benefits that the PN initial data could bring in bridging the fields of numerical and analytical relativity, we have introduced a hybrid approach to the initial data evaluation. We were able to significantly reduce the unphysical horizon mass loss, as well as reduce the eccentricity present in the PN data in ADM-TT coordinates, both undesired features previously reported in [1]. The method consists of solving for the traditional Bowen-York puncture data conformal factor and using this conformal factor to rescale the ADM canonical quantities as they appear in the PN data. The high eccentricity still present in the data was reduced by the use of an attenuation function in the black-hole inner zone, effectively decreasing the contributions of the higher-order

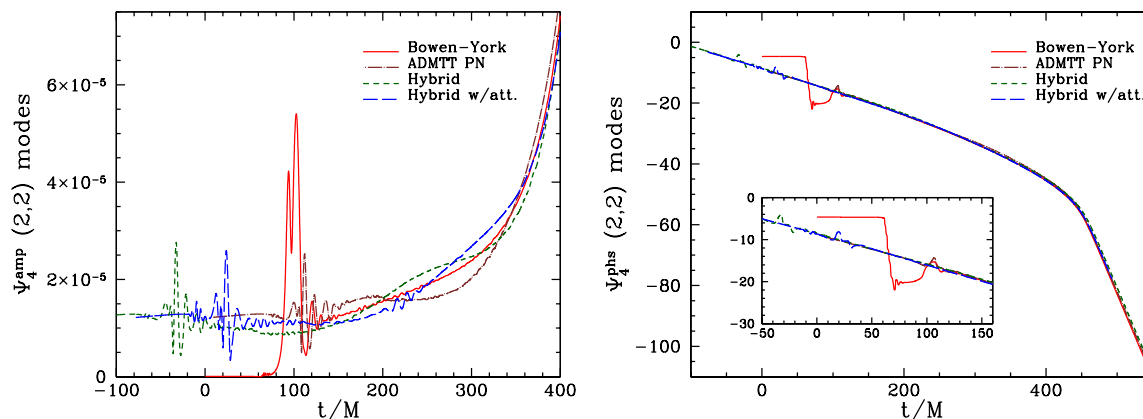


Figure 8. Comparison between the $\psi_4(2,2)$ mode amplitude (left) and phase (right) for the Bowen-York, ADM-TT PN, Hybrid and Hybrid with attenuation initial data. The extraction radius is $R_{\text{ext}} = 90M$.

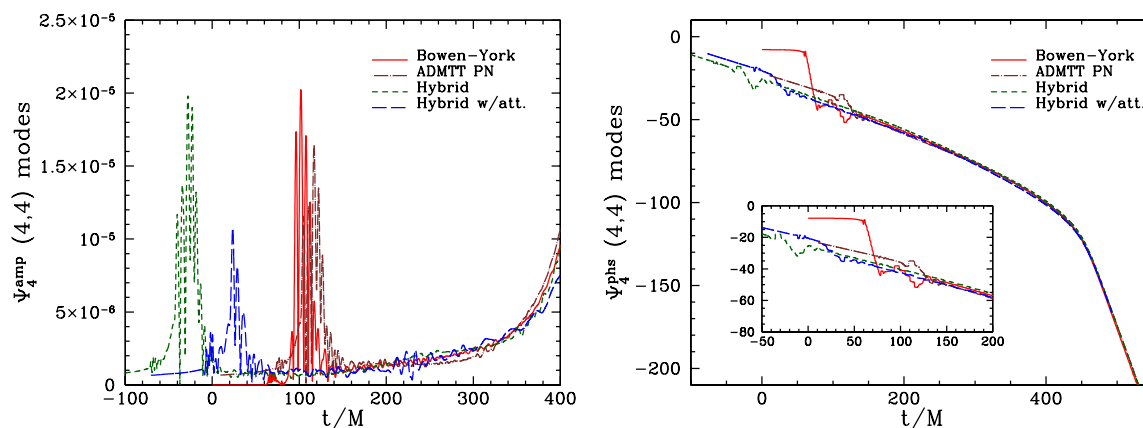


Figure 9. Comparison between the $\psi_4(4,4)$ mode amplitude (left) and phase (right) for the Bowen-York, ADM-TT PN, Hybrid and Hybrid with attenuation initial data. The extraction radius is $R_{\text{ext}} = 90M$.

PN terms and the transverse-traceless part of the metric to the canonical conjugate momentum and three-metric, respectively.

We plan to continue our studies with two lines of research. First, as a short-term project, we would like to reduce the eccentricity of the hybrid data even further by exploring different attenuation functions and by the iterative eccentricity reduction procedure described in Pfeiffer *et al* [84]. We plan to use larger orbital separations to facilitate this modeling and consequently the eccentricity reduction.

The second plan of research, a long-term one, is two-fold. On the analytic side, we would like to explore alternative analytic approximations to the metric and extrinsic curvature in the binary black-hole inner zones, where the point-particle approximation breaks down. Our plan is to match the PN metric to a perturbed, boosted Schwarzschild black hole, a la Yunes *et al* [85], with a trumpet topology in quasi-

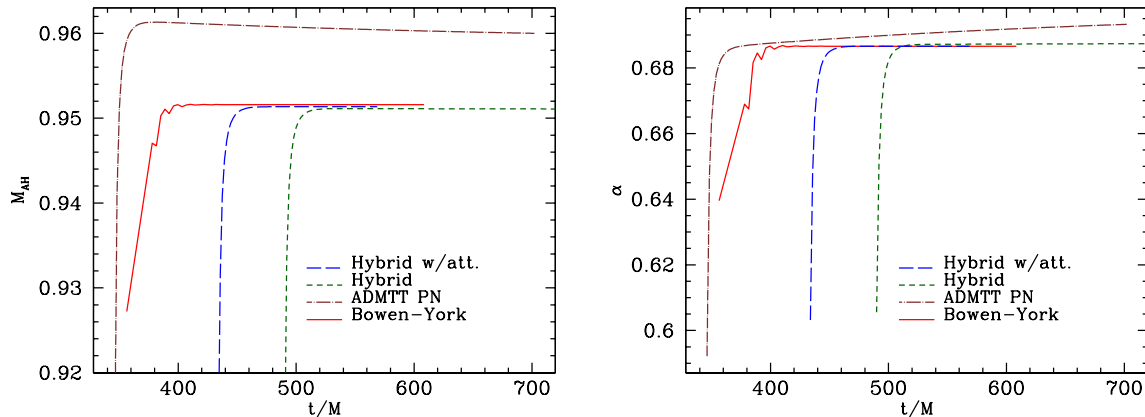


Figure 10. The apparent horizon mass and the dimensionless spin of the final black hole resulting from the evolutions of the Bowen-York, ADM-TT PN, Hybrid and Hybrid with attenuation initial data.

isotropic coordinates [86, 87, 88]; this should provide an analytic solution with smaller constraint violations. On the numerical side, we will implement a generic constraint solver for conformally curved data. By adopting a constraint-satisfying conformally curved metric we hope to better encode the past history of the binary and provide an initial data free of junk radiation.

Acknowledgments

We gratefully acknowledge the NSF for financial support from Grants No. PHY-0722315, No. PHY-0653303, No. PHY-0714388, No. PHY-0722703, No. DMS-0820923, No. PHY-0929114, No. PHY-0969855, No. PHY-0903782, No. CDI-1028087; and NASA for financial support from NASA Grants No. 07-ATFP07-0158 and No. HST-AR-11763. The authors acknowledge the Texas Advanced Computing Center (TACC) at The University of Texas at Austin for providing HPC resources that have contributed to the research results reported within this paper. URL: <http://www.tacc.utexas.edu>.

References

- [1] Kelly B J, Tichy W, Zlochower Y, Campanelli M and Whiting B F 2010 *Class. Quantum Grav.* **27** 114005 (*Preprint* [arXiv:0912.5311](https://arxiv.org/abs/0912.5311)[gr-qc])
- [2] Pretorius F 2005 *Phys. Rev. Lett.* **95** 121101 (*Preprint* [arXiv:gr-qc/0507014](https://arxiv.org/abs/gr-qc/0507014))
- [3] Campanelli M, Lousto C O, Marronetti P and Zlochower Y 2006 *Phys. Rev. Lett.* **96** 111101 (*Preprint* [arXiv:gr-qc/0511048](https://arxiv.org/abs/gr-qc/0511048))
- [4] Baker J G, Centrella J M, Choi D I, Koppitz M and van Meter J R 2006 *Phys. Rev. Lett.* **96** 111102 (*Preprint* [arXiv:gr-qc/0511103](https://arxiv.org/abs/gr-qc/0511103))
- [5] Campanelli M, Lousto C O and Zlochower Y 2006 *Phys. Rev. D* **74** 041501(R) (*Preprint* [arXiv:gr-qc/0604012](https://arxiv.org/abs/gr-qc/0604012))
- [6] Campanelli M, Lousto C O and Zlochower Y 2006 *Phys. Rev. D* **74** 084023 (*Preprint* [arXiv:astro-ph/0608275](https://arxiv.org/abs/astro-ph/0608275))

- [7] Campanelli M, Lousto C O, Zlochower Y, Krishnan B and Merritt D 2007 *Phys. Rev. D* **75** 064030 (*Preprint* [arXiv:gr-qc/0612076](#))
- [8] Herrmann F, Hinder I, Shoemaker D M, Laguna P and Matzner R A 2007 *Phys. Rev. D* **76** 084032 (*Preprint* [arXiv:0706.2541\[gr-qc\]](#))
- [9] Marronetti P *et al.* 2007 *Class. Quant. Grav.* **24** S43–S58 (*Preprint* [gr-qc/0701123](#))
- [10] Marronetti P, Tichy W, Brüggmann B, Gonzalez J A and Sperhake U 2008 *Phys. Rev. D* **77** 064010 (*Preprint* [arXiv:0709.2160\[gr-qc\]](#))
- [11] Berti E, Cardoso V, Gonzalez J A, Sperhake U, Hannam M D, Husa S and Brüggmann B 2007 *Phys. Rev. D* **76** 064034 (*Preprint* [arXiv:gr-qc/0703053](#))
- [12] Herrmann F, Shoemaker D M and Laguna P 2007 *Class. Quantum Grav.* **24** S33–S42 (*Preprint* [arXiv:gr-qc/0601026](#))
- [13] Baker J G, Centrella J M, Choi D I, Koppitz M, van Meter J R and Miller M C 2006 *Astrophys. J.* **653** L93 (*Preprint* [arXiv:astro-ph/0603204](#))
- [14] Gonzalez J A, Sperhake U, Brüggmann B, Hannam M D and Husa S 2007 *Phys. Rev. Lett.* **98** 091101 (*Preprint* [arXiv:gr-qc/0610154](#))
- [15] Herrmann F, Hinder I, Shoemaker D M, Laguna P and Matzner R A 2007 *Astrophys. J.* **661** 430–436 (*Preprint* [arXiv:gr-qc/0701143](#))
- [16] Campanelli M, Lousto C O, Zlochower Y and Merritt D 2007 *Astrophys. J.* **659** L5–L8 (*Preprint* [arXiv:gr-qc/0701164](#))
- [17] Campanelli M, Lousto C O, Zlochower Y and Merritt D 2007 *Phys. Rev. Lett.* **98** 231102 (*Preprint* [arXiv:gr-qc/0702133](#))
- [18] Lousto C O and Zlochower Y 2009 *Phys. Rev. D* **79** 064018 (*Preprint* [arXiv:0805.0159\[gr-qc\]](#))
- [19] Pollney D, Reisswig C, Rezzolla L, Szilágyi B, Ansorg M, Deris B, Diener P, Dorband E N, Koppitz M, Nagar A and Schnetter E 2007 *Phys. Rev. D* **76** 124002 (*Preprint* [arXiv:0707.2559\[gr-qc\]](#))
- [20] Gonzalez J A, Hannam M D, Sperhake U, Brüggmann B and Husa S 2007 *Phys. Rev. Lett.* **98** 231101 (*Preprint* [arXiv:gr-qc/0702052](#))
- [21] Brüggmann B, Gonzalez J A, Hannam M D, Husa S and Sperhake U 2008 *Phys. Rev. D* **77** 124047 (*Preprint* [arXiv:0707.0135\[gr-qc\]](#))
- [22] Choi D I, Kelly B J, Boggs W D, Baker J G, Centrella J M and van Meter J R 2007 *Phys. Rev. D* **76** 104026 (*Preprint* [arXiv:gr-qc/0702016](#))
- [23] Baker J G, Boggs W D, Centrella J M, Kelly B J, McWilliams S T, Miller M C and van Meter J R 2007 *Astrophys. J.* **668** 1140–1144 (*Preprint* [arXiv:astro-ph/0702390](#))
- [24] Schnittman J D, Buonanno A, van Meter J R, Baker J G, Boggs W D, Centrella J M, Kelly B J and McWilliams S T 2008 *Phys. Rev. D* **77** 044031 (*Preprint* [arXiv:0707.0301\[gr-qc\]](#))
- [25] Baker J G, Boggs W D, Centrella J M, Kelly B J, McWilliams S T, Miller M C and van Meter J R 2008 *Astrophys. J.* **682** L29–L32 (*Preprint* [arXiv:0802.0416\[astro-ph\]](#))
- [26] Healy J, Herrmann F, Hinder I, Shoemaker D M, Laguna P and Matzner R A 2009 *Phys. Rev. Lett.* **102** 041101 (*Preprint* [arXiv:0807.3292\[gr-qc\]](#))
- [27] Herrmann F, Hinder I, Shoemaker D M and Laguna P 2007 *Class. Quantum Grav.* **24** S33–S42
- [28] Tichy W and Marronetti P 2007 *Phys. Rev. D* **76** 061502(R) (*Preprint* [arXiv:gr-qc/0703075](#))
- [29] Koppitz M, Pollney D, Reisswig C, Rezzolla L, Thornburg J, Diener P and Schnetter E 2007 *Phys. Rev. Lett.* **99** 041102 (*Preprint* [arXiv:gr-qc/0701163](#))
- [30] Miller S H and Matzner R A 2009 *Gen. Rel. Grav.* **41** 525–539 (*Preprint* [arXiv:0807.3028\[gr-qc\]](#))
- [31] Boyle L, Kesden M and Nissanke S 2008 *Phys. Rev. Lett.* **100** 151101 (*Preprint* [arXiv:0709.0299\[gr-qc\]](#))
- [32] Boyle L and Kesden M 2008 *Phys. Rev. D* **78** 024017 (*Preprint* [arXiv:0712.2819\[astro-ph\]](#))
- [33] Buonanno A, Kidder L E and Lehner L 2008 *Phys. Rev. D* **77** 026004 (*Preprint* [arXiv:0709.3839\[astro-ph\]](#))

- [34] Tichy W and Marronetti P 2008 *Phys. Rev. D* **78** 081501(R) (*Preprint* {arXiv}:0807.2985[gr-qc])
- [35] Kesden M 2008 *Phys. Rev. D* **78** 084030 (*Preprint* {arXiv}:0807.3043[gr-qc])
- [36] Barausse E and Rezzolla L 2009 *Astrophys. J.* **704** L40–L44 (*Preprint* {arXiv}:0904.2577[gr-qc])
- [37] Rezzolla L 2009 *Class. Quantum Grav.* **26** 094023 (*Preprint* {arXiv}:0812.2325[gr-qc])
- [38] Lousto C O, Campanelli M, Zlochower Y and Nakano H 2010 *Class. Quantum Grav.* **27** 114006 (*Preprint* arXiv:0904.3541[gr-qc])
- [39] Buonanno A, Cook G B and Pretorius F 2007 *Phys. Rev. D* **75** 124018 (*Preprint* {arXiv}:gr-qc/0610122)
- [40] Baker J G, van Meter J R, McWilliams S T, Centrella J M and Kelly B J 2007 *Phys. Rev. Lett.* **99** 181101 (*Preprint* {arXiv}:gr-qc/0612024)
- [41] Pan Y, Buonanno A, Baker J G, Centrella J M, Kelly B J, McWilliams S T, Pretorius F and van Meter J R 2008 *Phys. Rev. D* **77** 024014 (*Preprint* {arXiv}:0704.1964[gr-qc])
- [42] Buonanno A, Pan Y, Baker J G, Centrella J M, Kelly B J, McWilliams S T and van Meter J R 2007 *Phys. Rev. D* **76** 104049 (*Preprint* {arXiv}:0706.3732[gr-qc])
- [43] Hannam M D, Husa S, Sperhake U, Brüggmann B and Gonzalez J A 2007 *Phys. Rev. D* **77** 044020 (*Preprint* {arXiv}:0706.1305[gr-qc])
- [44] Hannam M D, Husa S, Brüggmann B and Gopakumar A 2008 *Phys. Rev. D* **78** 104007 (*Preprint* {arXiv}:0712.3787[gr-qc])
- [45] Gopakumar A, Hannam M D, Husa S and Brüggmann B 2008 *Phys. Rev. D* **78** 064026 (*Preprint* {arXiv}:0712.3737[gr-qc])
- [46] Hinder I, Herrmann F, Laguna P and Shoemaker D 2008 Comparisons of eccentric binary black hole simulations with post-Newtonian models arXiv:0806.1037 [gr-qc]
- [47] Campanelli M, Lousto C O, Nakano H and Zlochower Y 2009 *Phys. Rev. D* **79** 084010 (*Preprint* {arXiv}:0808.0713[gr-qc])
- [48] Abbott B P *et al.* (LIGO Scientific) 2009 *Rep. Prog. Phys.* **72** 076901 (*Preprint* {arXiv}:0711.3041[gr-qc])
- [49] Acernese F *et al.* 2008 *Class. Quantum Grav.* **25** 114045
- [50] Kuroda K and LCGT Collaboration 2010 *Class. Quantum Grav.* **27** 084004
- [51] Danzmann K, Bender P, Brillet A, Cruise I C A, Cutler C, Fidecaro F, Folkner W, Hough J, McNamara P, Peterseim M, Robertson D, Rodrigues M, Rüdiger A, Sandford M, Schäfer G, Schilling R, Schutz B F, Speake C, Stebbins R, Sumner T, Touboul P, Vinet J Y, Vitale S, Ward H and Winkler W 1998 LISA pre-phase A report, 2nd ed. Tech. rep. Max-Planck-Institut für Quantenoptik MPQ 233
- [52] Punturo M *et al.* 2010 *Class. Quantum Grav.* **27** 194002
- [53] Ando M *et al.* 2010 *Class. Quantum Grav.* **27** 084010
- [54] Bowen J M and York J W 1980 *Phys. Rev. D* **21** 2047–2056
- [55] Brandt S R and Brüggmann B 1997 *Phys. Rev. Lett.* **78** 3606–3609 (*Preprint* {arXiv}:gr-qc/9703066)
- [56] Tichy W, Brüggmann B, Campanelli M and Diener P 2003 *Phys. Rev. D* **67** 064008 (*Preprint* {arXiv}:gr-qc/0207011)
- [57] Kelly B J, Tichy W, Campanelli M and Whiting B F 2007 *Phys. Rev. D* **76** 024008 (*Preprint* arXiv:0704.0628[gr-qc])
- [58] Blanchet L 2006 *Living Rev. Relativity* **9** <http://www.livingreviews.org/lrr-2006-4> (*Preprint* {arXiv}:gr-qc/0202016)
- [59] Schäfer G 2010 *Mass and Motion in General Relativity* Fundamental Theories of Physics ed Blanchet L, Spallicci A and Whiting B (New York: Springer) proceedings of the C.N.R.S. “School on Mass” in Orléans, France, June 2008 (*Preprint* {arXiv}:0910.2857[gr-qc])
- [60] Ohta T, Okamura H, Kimura T and Hiida K 1973 *Prog. Theor. Phys.* **50** 492–514
- [61] Ohta T, Okamura H, Hiida K and Kimura T 1974 *Prog. Theor. Phys.* **51** 1220–1238

- [62] Ohta T, Okamura H, Kimura T and Hiida K 1974 *Prog. Theor. Phys.* **51** 1598–1612
- [63] Schäfer G 1985 *Ann. Phys.* **161** 81–100
- [64] Damour T and Schäfer G 1985 *Gen. Rel. Grav.* **17** 879–905
- [65] Schäfer G 1986 *Gen. Rel. Grav.* **18** 255–270
- [66] Jaranowski P and Schäfer G 1998 *Phys. Rev. D* **57** 7274–7291 Erratum: *ibid.* **63**, 029902(E) (2001) (Preprint [arXiv:gr-qc/9712075](https://arxiv.org/abs/gr-qc/9712075))
- [67] Buonanno A, Chen Y and Damour T 2006 *Phys. Rev. D* **74** 104005 (Preprint [arXiv:gr-qc/0508067](https://arxiv.org/abs/gr-qc/0508067))
- [68] Brill D R and Lindquist R W 1963 *Phys. Rev.* **131** 471–476
- [69] Johnson-McDaniel N K, Yunes N, Tichy W and Owen B J 2009 *Phys. Rev. D* **80** 124039 (Preprint [arXiv:0907.0891](https://arxiv.org/abs/0907.0891)[gr-qc])
- [70] Detweiler S L 2005 *Class. Quantum Grav.* **22** S681–S716 (Preprint [gr-qc/0501004](https://arxiv.org/abs/gr-qc/0501004))
- [71] Ansorg M, Brügmann B and Tichy W 2004 *Phys. Rev. D* **70** 064011 (Preprint [arXiv:gr-qc/0404056](https://arxiv.org/abs/gr-qc/0404056))
- [72] Zlochower Y, Baker J G, Campanelli M and Lousto C O 2005 *Phys. Rev. D* **72** 024021 (Preprint [arXiv:gr-qc/0505055](https://arxiv.org/abs/gr-qc/0505055))
- [73] Lousto C O and Zlochower Y 2008 *Phys. Rev. D* **77** 024034 (Preprint [arXiv:0711.1165](https://arxiv.org/abs/0711.1165)[gr-qc])
- [74] Alcubierre M, Brügmann B, Diener P, Koppitz M, Pollney D, Seidel E and Takahashi R 2003 *Phys. Rev. D* **67** 084023 (Preprint [arXiv:gr-qc/0206072](https://arxiv.org/abs/gr-qc/0206072))
- [75] Cactus Computational Toolkit home page: <http://www.cactuscode.org>
- [76] Einstein Toolkit web page: <http://www.einsteintoolkit.org>
- [77] Schnetter E, Hawley S H and Hawke I 2004 *Class. Quantum Grav.* **21** 1465–1488 (Preprint [arXiv:gr-qc/0310042](https://arxiv.org/abs/gr-qc/0310042))
- [78] Thornburg J 2004 *Class. Quantum Grav.* **21** 743–766 (Preprint [arXiv:gr-qc/0306056](https://arxiv.org/abs/gr-qc/0306056))
- [79] Dreyer O, Krishnan B, Shoemaker D M and Schnetter E 2002 *Phys. Rev. D* **67** 024018 (Preprint [arXiv:gr-qc/0206008](https://arxiv.org/abs/gr-qc/0206008))
- [80] Christodoulou D 1970 *Phys. Rev. Lett.* **25** 1596–1597
- [81] Numerical Relativity and Analytical Relativity (NRAR) Home Page <https://www.ninja-project.org/doku.php?id=nrar:home>
- [82] Mroué A H, Pfeiffer H P, Kidder L E and Teukolsky S A 2010 Measuring orbital eccentricity and periastron advance in quasi-circular black hole simulations [arXiv:1004.4697](https://arxiv.org/abs/1004.4697) [gr-qc]
- [83] Tichy W and Marronetti P 2010 A simple method to set up low eccentricity initial data for moving puncture simulations [arXiv:1010.2936](https://arxiv.org/abs/1010.2936) [gr-qc]
- [84] Pfeiffer H P, Brown D A, Kidder L E, Lindblom L, Lovelace G and Scheel M A 2007 *Class. Quantum Grav.* **24** S59–S82 (Preprint [arXiv:gr-qc/0702106](https://arxiv.org/abs/gr-qc/0702106))
- [85] Yunes N, Tichy W, Owen B J and Brügmann B 2006 *Phys. Rev. D* **74** 064013 (Preprint [arXiv:gr-qc/0601046](https://arxiv.org/abs/gr-qc/0601046))
- [86] Hannam M D, Husa S, Ohme F, Brügmann B and Ó Murchadha N 2008 *Phys. Rev. D* **78** 064020 (Preprint [arXiv:0804.0628](https://arxiv.org/abs/0804.0628)[gr-qc])
- [87] Hannam M D, Husa S and Ó Murchadha N 2009 *Phys. Rev. D* **80** 124007 (Preprint [arXiv:0908.1063](https://arxiv.org/abs/0908.1063)[gr-qc])
- [88] Immerman J D and Baumgarte T W 2009 *Phys. Rev. D* **80** 061501(R) (Preprint [arXiv:0908.0337](https://arxiv.org/abs/0908.0337)[gr-qc])